

Water harvest via dewing

Anna Lee,[†] Myoung-Woon Moon,[‡] Hyuneui Lim,[§] Wan-Doo Kim,[§] and Ho-Young Kim^{*,†}

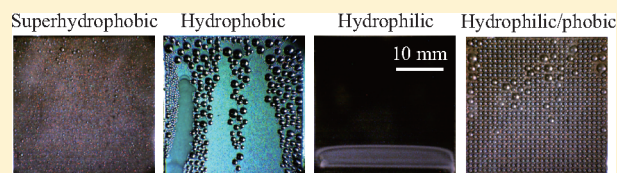
[†]School of Mechanical and Aerospace Engineering, Seoul National University, Seoul 151-744, Korea

[‡]Interdisciplinary Matters Convergence Institute, Korea Institute of Science and Technology, Seoul 136-791, Korea

[§]Department of Nature-Inspired Nanoconvergence Systems, Korea Institute of Machinery and Materials, Daejeon 305-343, Korea

ABSTRACT: Harvesting water from humid air via dewing can provide a viable solution to a water shortage problem where liquid-phase water is not available. Here we experimentally quantify the effects of wettability and geometry of the condensation substrate on the water harvest efficiency. Uniformly hydrophilic surfaces are found to exhibit higher rates of water condensation and collection than surfaces with lower wettability.

This is in contrast to a fog basking method where the most efficient surface consists of hydrophilic islands surrounded by hydrophobic background. A thin drainage path in the lower portion of the condensation substrate is revealed to greatly enhance the water collection efficiency. The optimal surface conditions found in this work can be used to design a practical device that harvests water as its biological counterpart, a green tree frog, *Litoria caerulea*, does during the dry season in tropical northern Australia.



I. INTRODUCTION

A water shortage has been a major problem faced by the modern civilization in both arid and humid environments.^{1,2} Collecting water out of foggy wind was recently suggested as one of its remedies. Motivated by the fog basking behavior of beetles in the Namib Desert,³ biomimetic approaches to harvest water from tiny water droplets dispersed in the air have been investigated.^{4–8} Parker and Lawrence⁴ reported that the *Stenocara* beetle's back was covered with an array of hydrophilic bumps surrounded by hydrophobic background, which was supposed to facilitate water collection. Garrod et al.⁶ measured the water-collection efficiency of the wettability-patterned surfaces to find the optimal diameter of hydrophilic spots in the hydrophobic background. Dorrer and Rühle⁷ obtained the critical volume of water to initiate the sliding of drops captured on circular hydrophilic area surrounded by superhydrophobic surface. Later, it turned out that it is *Onymacris unguicularis*, not *Stenocara* sp., that collects water through fog basking and that all the four species of the Namib Desert beetles, *Stenocara gracilipes*, *O. unguicularis*, *Onymacris laeviceps* and *Physasteria cribripes*, possess uniformly hydrophobic backs without hydrophilic islands.⁸ However, the fact that hydrophilic–hydrophobic surface patterns exhibit superior water collection performance to surfaces with uniform wettability, either hydrophilic or hydrophobic, is now well established.

While the fog basking resorts to airborne droplets which are already in a liquid state and carried with wind, harvesting water from unsaturated air, which has more general implications, requires a different approach. That is, humid air needs to be cooled down to the dew point for water vapor to condense into liquid water. Such a water collection scheme was found to be adopted by green tree frogs, *Litoria caerulea*, in tropical northern Australia.⁹ In the dry season, the frogs that are cooled during nighttime return to a warm humid tree hollow where

water condensation occurs on their body surface. Images of drops condensed on the body surface reveal that the apparent contact angle is approximately 40° and that they easily spread into a film on wrinkled regions. It was also suggested that the Australian desert lizards, *Moloch horridus*, may collect water on its skin as vapor condenses due to severe temperature difference of more than 30 °C between day and night.¹⁰ Their body surfaces were reported to exhibit superhydrophilic nature owing to micro-ornamentation on the outer surface of the scales.¹¹

Since such vapor condensation occurs on cold surfaces, a question naturally arises of the optimal wettability and geometry of the condensation substrate to maximize the water collection efficiency. In the field of heat transfer, condensation on cold surfaces has been widely studied for applications in HVAC (heating, ventilation and air-conditioning) systems. The effects of frontal velocity of air,^{12,13} and wettability^{13–16} and topography^{12,16–18} of the heat exchanger surfaces on the condensation heat transfer coefficient were investigated. However, most heat exchangers possess complicated shapes, e.g. shell-and-tube, pin-fin, etc., because they are concerned with effective heat transfer between the liquid flowing in the tube and the surrounding air.¹⁹ Further, enhancing the collection efficiency of liquid-phase water on the outer surface of heat exchangers has rarely drawn significant scientific interest. Therefore, the results of the conventional condensation heat exchanger studies cannot be directly applied to the design of water harvesting systems.

Condensation corresponds to the removal of the latent heat of vapor by a cold surface where the heterogeneous nucleation

Received: April 5, 2012

Revised: June 9, 2012

Published: June 25, 2012

occurs.²⁰ The condensed water covers the solid surface, which acts as a thermal resistance between the air and the cold surface. Previous studies reported enhanced heat transfer from a heat exchanger surface with either hydrophilic²¹ or hydrophobic coatings.²² Hydrophilic coatings promote the heterogeneous nucleation and lower the thermal resistance by forming a thin liquid film on the surface (filmwise condensation). On hydrophobic surfaces where dropwise condensation occurs,^{23,24} condensed drops can be easily removed from the surface by gravity and air streams; thus, the thermal resistance can be lowered. On the other hand, the aforementioned fog basking studies revealed that hydrophilic–hydrophobic wettability patterns can enhance the water collection efficiency.⁶ Therefore, here we investigate the effects of the cold surface's wettability on the efficiency of water harvest via dewing. Then we vary the geometry of cold surface aiming to facilitate the transfer of condensed water onto a collector, upon which a practical water collection efficiency critically depends.

II. EXPERIMENTAL SECTION

Figure 1 shows the experimental apparatus where a transparent acrylic chamber houses a flat condensation substrate placed on a thermo-

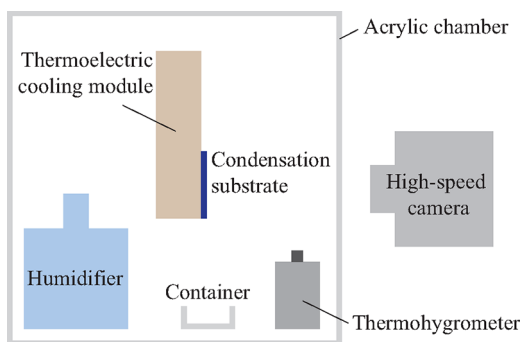


Figure 1. Experimental setup for harvesting water via condensation.

electric cooling module. A commercial humidifier introduces fog into the chamber, which is vaporized in the air and then condenses back to liquid water on the cold surface. The experiments were performed with the temperature and humidity inside the chamber maintained at 25.0 ± 1.0 °C and 90–95%, respectively, as measured by a thermohygrometer. The temperature of the condensation substrate, measured by an attached thermocouple, is kept at 10.0 ± 0.2 °C, lower than the dew point 22–25 °C, by controlling the cooling module. Liquid water condensed on the vertically situated cold surface drains into a container by gravity. The experiments started with cooling the condensation substrate as the humidity inside the chamber having already reached 90%. A high-speed camera imaged the condensation behavior. In 2 h, the weight of water collected at the container and that retained on the cold surface were measured.

As the condensation substrates, we used a square silicon wafer with $L = 30$ mm in sidelength for its high thermal conductivity and ease of wettability and roughness control. We obtained the “as-placed” contact angle, θ_s , of deionized (DI) water on the horizontal solid surfaces by measuring the angle between the tangential lines of the liquid interface and the solid surface at the contact line of a sessile drop with $5 \mu\text{L}$ in volume. The critical advancing contact angle, θ_a , and the critical receding contact angle, θ_r , were measured by increasing (θ_a) or decreasing (θ_r) the drop volume until the contact line starts to move with an aid of a syringe needle immersed in the drop.²⁶ We tested five different types of surfaces: superhydrophobic, moderately hydrophobic, smooth hydrophilic, rough hydrophilic (i.e., superhydrophilic), and superhydrophilic–superhydrophobic patterned surface. For a superhydrophobic surface, the silicon wafer was first etched by CF_4

plasma for 90 min to attain nanoscale roughness, immersed in DI water for 1 min, dried by N_2 gas. Then it was coated with a hexamethyldisiloxane (HMDSO) film having a low surface energy and long-term stability.^{27,28} A moderately hydrophobic surface was prepared by coating with the vapor of solution of mineral oil and decyltrichlorosilane (DTS) with the weight ratio 7:5 for 3 min.²⁹ To make a smooth silicon wafer surface hydrophilic, the wafer was treated by air plasma for 3 min. A superhydrophilic surface was obtained by treating the foregoing superhydrophobic surface with air plasma for 3 min. We note that both the superhydrophobic and superhydrophilic surfaces can be mass-produced for practical applications using a large-scale plasma chamber.³⁰ The superhydrophilicity of the nanostructured surfaces lasts for over 20 days³¹ while the hydrophilicity vanishes in a few minutes on smooth surfaces when exposed to ambient air. Smooth silicon or glass surfaces can be made hydrophilic and remain so until contaminated by organic contaminations if cleaned with piranha solution. The contact angles for the surfaces used in this work are listed in Table 1.

Table 1. As-Placed (θ_s), Critical Advancing (θ_a), and Critical Receding (θ_r) Contact Angles for the Surfaces Used in the Experiments^a

surface	θ_s (deg)	θ_a (deg)	θ_r (deg)
I. superhydrophobic	162	164	161
II. moderately hydrophobic	105	106	84
III. hydrophilic	3	4	0
IV. superhydrophilic	1	2	0
V. superhydrophilic/superhydrophobic	1/162	2/164	0/161

^aThe standard deviation is $\sim 1^\circ$. For surface V, the first and second angles in each entry correspond to the values in the superhydrophilic and superhydrophobic region, respectively.

The photolithography was employed to generate superhydrophilic–superhydrophobic patterns as illustrated in Figure 2a. The superhydrophobic surface was spin-coated with a photoresist AZ1512 for 10 s at 500 rpm and then for 45 s at 3000 rpm. After baking the wafer on a hot plate at 95 °C for 50 s, UV exposure was carried out with a photomask on the photoresist. The UV-exposed photoresist was removed and the exposed area was selectively treated with air plasma

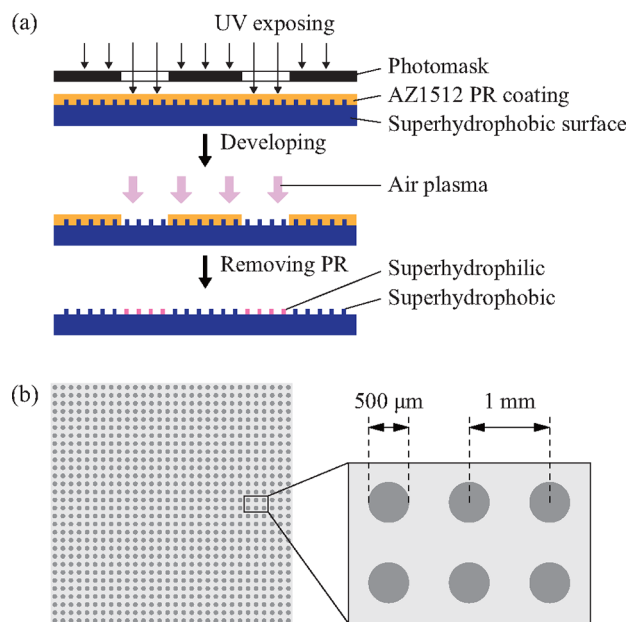


Figure 2. (a) Wettability patterning process via photolithography. (b) Schematic of a superhydrophilic–superhydrophobic pattern.

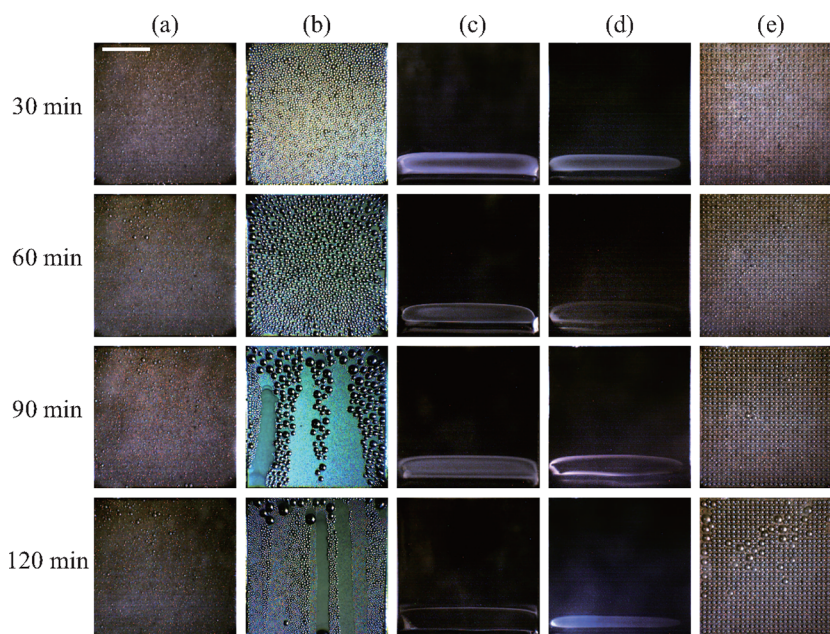


Figure 3. Condensation behavior of water vapor with time on (a) superhydrophobic, (b) moderately hydrophobic, (c) hydrophilic, (d) superhydrophilic, and (e) superhydrophilic–superhydrophobic patterned surfaces. Scale bar: 10 mm.

to become superhydrophilic. The unexposed area remained superhydrophobic after removing the photoresist with acetone. The pattern consists of a square array of superhydrophilic circles with 500 μm in diameter and 1 mm in pitch (distance between the centers), Figure 2b, which was reported to exhibit the highest water collection efficiency in fog basking.⁶

In addition to the condensation experiments, we tested the effects of the geometry of lower portion of the condensation surface on the drainage efficiency. As a drainage path, the lower portion of the wafer was patterned so that the superhydrophilic lane is surrounded by the superhydrophobic area. Although we photolithographically defined the hydrophilic lane using a photoresist, we note that a cheap film can replace photoresist in mass-production. To quickly measure the instantaneous weight of the wet substrate and the dripping water, we supplied water near the top edge of the substrate with a syringe instead of using the vapor-condensation setup. Drops of 2 μL in volume were dispensed from the needle thus the volume of the water film spread on the surface was increased in 2 μL increments. A care was taken not to disturb the film so that the gravity can still dominantly drive the downward flow. Immediately after a drop of water falls off the surface into a container, the weights of the drop and residing water on the surface were measured to determine the minimum and maximum water retention capacity of each surface design.

III. RESULTS AND DISCUSSION

A. Water Collection by Condensation. The condensation behaviors of the surfaces with different wettability and roughness are compared in Figure 3. On the superhydrophobic surface, tiny droplets emerge on the surface, which is termed dropwise condensation, as shown in Figure 3a. They roll down the vertical surface due to gravity when their diameter reaches about 0.3 mm and are collected at the container underneath the condensation substrate. The maximum size of a drop that can adhere to a vertical surface can be determined by balancing the capillary force owing to the contact angle hysteresis (the difference between θ_a and θ_r) with the gravitational force^{32,33}

$$b\sigma(\cos \theta_r - \cos \theta_a) = \rho g V \quad (1)$$

where b is the maximum diameter of the contact area of the drop with the solid surface, σ and ρ are the surface tension and

the density of the water, respectively, g is the gravitational acceleration and V is the volume of the drop. Assuming that the drop assumes a spherical cap shape, b and V can be related as:

$$V = \frac{\pi b^3}{24} (2\csc^3 \theta_s - 3\cot \theta_s \csc^2 \theta_s + \cot^3 \theta_s) \quad (2)$$

Using the contact angle values in Table 1, we find the maximum volume of the water drop that can adhere to surface I to be $9.35 \times 10^{-12} \text{ m}^3$, giving the nominal diameter of the corresponding spherical cap as 0.26 mm, consistent with our experimental observations (0.3 mm). On the moderately hydrophobic surface (II), dropwise condensation still occurs as shown in Figure 3b. Unlike those on the superhydrophobic surface, the droplets tend to coalesce during growth because they do not fall off the surface as easily. A droplet starts to slide down the surface when its base diameter reaches approximately 2.9 mm after several coalescence events, which is consistent with the calculation result using eq 1 and the contact angles in Table 1, $b = 2.64 \text{ mm}$. The drop that slides down the surface further merges with the drops in its way thus accelerates before entering the container.

On both hydrophilic, Figure 3c, and superhydrophilic, Figure 3d, surfaces, a thin layer of liquid water is formed as soon as the substrates are cooled down, which is termed filmwise condensation. This reveals that micro- and nanoscale roughness structures on hydrophilic surfaces play unimportant roles in determining the condensation behavior because the small roughness is immediately covered by a water film. The liquid water flows down the vertical surface due to gravity, but stops at the bottom of the cold surface to form a liquid puddle unlike the droplets on the foregoing hydrophobic surfaces that have sufficient kinetic energy to overcome the edge effect. The puddle's contact line is pinned at the bottom edge of the substrate³⁴ as illustrated in Figure 4. As the puddle volume increases to a critical value, the puddle drips. Our observation indicates that the puddle falls off the substrate when its maximum cross-sectional area (when viewed from the side) reaches approximately 14 mm^2 as obtained by the digital image

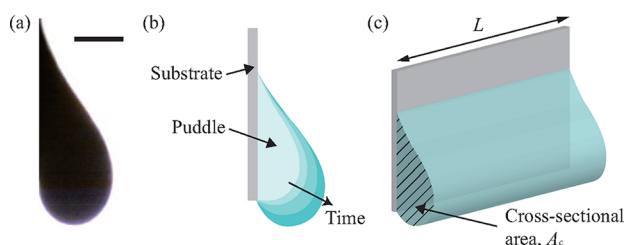


Figure 4. (a) Image of the side of a puddle at the bottom edge of the hydrophilic condensation substrate. Scale bar: 2 mm. (b) Schematic of the side view of the puddle. (c) Cross-sectional area of the puddle uniform along the substrate width.

analysis. We rationalize this result by a simple scaling concept. We first note that θ_a approaches 180° while θ_r is 0 due to the contact line pinning. We assume a uniform cross-sectional area along the plate edge as illustrated in Figure 4c. Balancing the gravitational force on the puddle, $\rho g A_c L$, with the capillary force, $2\sigma L$, where A_c is the cross-sectional area of the puddle upon dripping, leads to $A_c \approx 2\sigma/(\rho g) = 14.7 \text{ mm}^2$, consistent with our experimental observation. Here we have neglected the surface tension force along the side edge of the puddle because it is perpendicular to the gravitational direction and its length is insignificant compared with L .

On the superhydrophilic–superhydrophobic patterned surface, the superhydrophilic circles are easily wet by water film but the superhydrophobic background only collects tiny droplets. Sessile drops grow in size on the superhydrophilic islands but seldom slide down the surface, which is due to the extreme difference of θ_a and θ_r on the patterned surface. The drop meets the superhydrophobic surface at the front thus θ_a approaches 180° while it is pulled by the superhydrophilic surface in the rear thus $\theta_r \approx 0$. Therefore, the drop volume should grow to V_c to overcome the contact angle hysteresis: $V_c \approx 2a\sigma/(\rho g) = 7.35 \text{ }\mu\text{L}$, where a is the diameter of the superhydrophilic circle, $500 \text{ }\mu\text{m}$. As the thermal resistance between the cold substrate and the surrounding air increases with the growth of the drop thickness, it is almost impossible for the drops on the patterned surface to grow to V_c as explained in the following.

We first estimate the time for the drop to grow to V_c assuming that the surrounding gas is pure water vapor. The thermal resistance associated with the heat transfer between the cold substrate and water vapor is given by³⁵

$$R = \frac{1}{\pi r^2} \frac{1}{1 - r_m/r} \left[\frac{r\theta}{4k_l \sin \theta} + \frac{1}{2h_i(1 - \cos \theta)} \right] \quad (3)$$

where r is the radius of drop, θ is the instantaneous apparent contact angle of the growing drop, k_l is the thermal conductivity of condensate and h_i is the interfacial heat transfer coefficient, which varies from $0.383 \text{ MW m}^{-2} \text{ K}^{-1}$ to $15.7 \text{ MW m}^{-2} \text{ K}^{-1}$ for a vapor pressure ranging from 0.01 to 1.0 atm.³⁶ The minimum viable drop radius, r_m is given by $r_m = 2\sigma T_s/(h_{fg}\rho\Delta T)$,³⁷ where T_s is the vapor saturation temperature (297 K), $\Delta T = T_s - T_w$ with T_w being the wall temperature, and h_{fg} is the latent heat of condensation at the bulk air temperature, T_∞ . The model assumes that the gas–liquid interface temperature is given by the saturation temperature of water vapor. The time t_c for a drop to grow to reach the volume V_c can be calculated by integrating the following energy equation:

$$\rho h_{fg} \frac{dV}{dt} = \frac{\Delta T}{R} \quad (4)$$

The volume change dV can be expressed as

$$dV = A_s d\epsilon \quad (5)$$

where $A_s = (\pi/2)a^2(1 - \cos\theta)/\sin^2\theta$ is the gas–liquid interfacial area and $d\epsilon = (1/4)a(\csc^2\theta - \cot\theta \csc\theta)d\theta$ is the mean displacement of A_s .³⁵ Then the critical time is given by

$$\begin{aligned} t_c &= \int_0^{\epsilon(\theta_c)} \rho h_{fg} \frac{RA_s}{\Delta T} d\epsilon \\ &= \frac{\rho h_{fg}}{\Delta T} \int_0^{\theta_c} \frac{a}{16} \frac{1 - \cos \theta}{\sin^2 \theta} \left(\frac{a\theta}{k_l} \frac{1 - \cos \theta}{\sin^2 \theta} + \frac{4}{h_i} \right) \\ &\quad \frac{1}{1 - 2(r_m/a)\sin \theta} d\theta \end{aligned} \quad (6)$$

where θ_c is θ at t_c . Substituting the properties of water, t_c is calculated to be approximately 32 min. While this model assumes the gas to be pure water vapor, the real surrounding gas is an air–vapor mixture. Because the concentration of vapor near the gas–liquid interface is lower than in the bulk humid air due to the resistance of the air–vapor boundary layer, the gas–liquid interface temperature is lower than the saturation temperature of pure water vapor.^{20,36} When the mass fraction of water vapor in gas is 90%, the heat transfer rate was measured to be reduced to 10% of the value corresponding to the pure water vapor.³⁸ This indicates the strong effects of the unsaturated air mixture on the interfacial heat transfer. Considering that the mass fraction of water vapor in saturated air at room temperature is at most 3%, the reduction in the heat transfer rate must be much greater. In consequence, the time for a drop to grow to V_c in volume is much longer than 32 min and the duration of our experiment (2 h). Thus, only droplets formed on superhydrophobic portions can be collected in the container while ones on superhydrophilic areas adhere to the surface.

This finding is in stark contrast to the results of the fog basking experiments that the wettability patterned surfaces have a water collection efficiency higher than surfaces of uniform wettability.⁶ The reasoning for these contrasting results is as follows. In fog basking, water droplets should be conveyed onto the substrate by air stream—the average wind speed is reported to be 5 m/s in the Namib desert,⁴ and the wind was actively blown to the substrate at the rate of 11 L/min in the experiments of Garrod et al.⁶ As the volume of sessile drops grows, the surface area that can capture tiny airborne droplets increases. Then the drop can easily reach V_c in volume on hydrophilic islands, which can effectively roll off the superhydrophobic background. However, in our dewing experiments where the ambient air is still, drops grow very slowly and hardly fall off the hydrophilic islands because the drop growth depends only on thermal diffusion between humid air and the substrate.

Figure 5a shows the rates of water collection and condensation for each surface. The water collection rate, η_b , is obtained by dividing the weight of the water collected at the container by the duration of the experiment. For the condensation rate, η_m , the weight of water remaining on the substrate is added to that of the collected water and then the total water weight is divided by the time. We see that the hydrophilic surface (III) shows the highest rates for both water collection and total condensation. The rates decrease as the

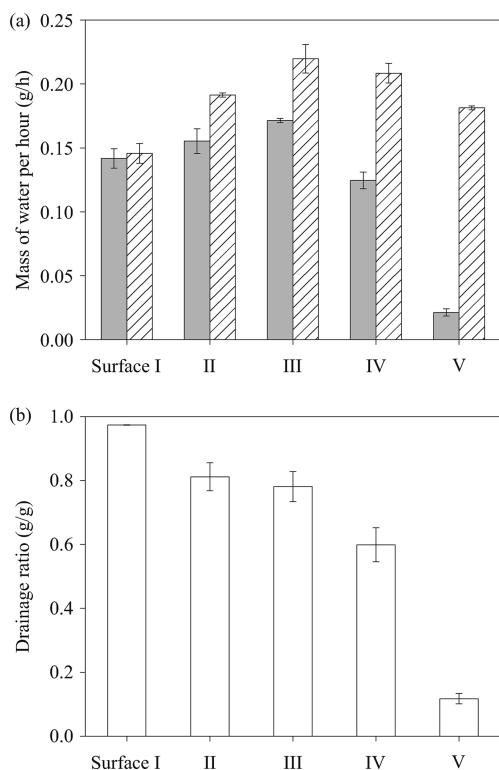


Figure 5. (a) Water collection rate (gray bar) and condensation rate (hatched bar) of the square wafers of differing wettability. (b) Drainage ratio, i.e., the amount of water actually collected divided by the total amount of water condensed. The surface number follows that of Table 1.

surface wettability gets weaker, with the superhydrophobic surface (I) having the lowest rates. The condensation rate of the superhydrophilic surface (IV) is similar to that of the hydrophilic surface (III), but the collection rate is lower. Although the detailed fluid-dynamic mechanism calls for more investigations, it is supposed to be because the rough hydrophilic surface is capable of holding water film on it more effectively due to increased friction than smooth surfaces. Thus, the drainage of the film is retarded on surface IV compared to surface III. The collection rate is the lowest for the hydrophilic–hydrophobic pattern (V) for the reason delineated above. But its condensation rate is similar to that of the moderately hydrophobic surface (II). It is reasonable considering that the condensation rate is governed by the surface wettability—surface V is composed of the hydrophilic areas of high condensation rate and the hydrophobic areas of low condensation rate.

The hydrophilic surfaces are superior in condensation rate from its early stage when the dry surfaces directly face humid air. The heterogeneous nucleation rate, J , is known to critically depend on the equilibrium contact angle, θ_e , as³⁹

$$J = J_0 \exp \left[-\pi \sigma r^{*2} \left(\frac{2 - 3 \cos \theta_e + \cos^3 \theta_e}{3 k_B T} \right) \right] \quad (7)$$

where J_0 is a kinetic constant, k_B is the Boltzmann constant and T is the absolute temperature. The critical radius, r^* , is given by $r^* = 2\sigma / [nk_B \ln(p/p_\infty)]$, where n is the number of molecules per unit volume of the liquid, p is the vapor pressure and p_∞ is the equilibrium vapor pressure above a flat surface of the condensed phase at temperature T . Figure 6 shows that J

normalized by its value at $\theta = 180^\circ$ decreases over tens of orders with the increase of the contact angle.

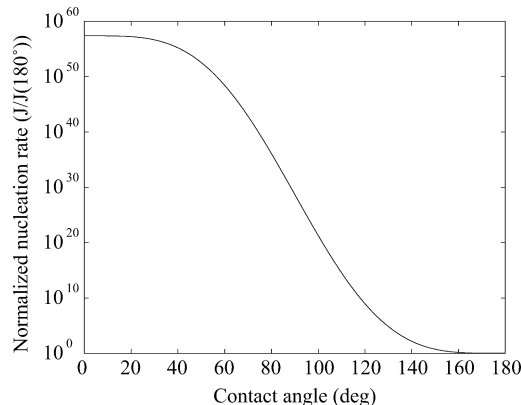


Figure 6. Theoretical heterogeneous nucleation rate versus contact angle. The normalized nucleation rate is plotted for the experimental condition.

On the superhydrophobic surface (I), tiny droplets easily roll off the surface all the way down to the container although the nucleation rate is quite low. Therefore, the drainage ratio, k , defined as the weight of water collected in a container to the total weight of water condensed ($k = \eta_l / \eta_n$) is the highest for the superhydrophilic–superhydrophobic pattern (V) is the lowest because large drops on the superhydrophilic islands keep stuck to the substrate.

The condensation rate of water film on the hydrophilic surface can be theoretically predicted. The steady-state energy balance of the system consisting of humid air and the liquid film contacting the cold substrate can be written as

$$q_v + q_L = q_d \quad (8)$$

where q_v , q_L , and q_d are the heat transfer rates per unit area associated with the convection in the humid air, the release of latent heat of water due to condensation, and the conduction through the liquid film, respectively. When the temperature of the gas–liquid interface is T_i , we get

$$q_v = h_v(T_\infty - T_i) \quad (9)$$

Here h_v is the average heat transfer coefficient for laminar free convection on a vertical surface, given by $Nu = h_v L / k_a = 0.68 + 0.67 Ra^{1/4} / [1 + (0.492 / Pr)^{9/16}]^{4/9}$,⁴⁰ where Nu is the average Nusselt number over the plate of length $L = 30$ mm and k_a is the thermal conductivity of air. Ra is the Rayleigh number defined as $Ra = g\beta(T_\infty - T_w)L^3 / (\nu\alpha)$, where β , ν and α is the thermal expansion coefficient, the kinematic viscosity and the thermal diffusivity of air, respectively. $Pr = \nu/\alpha$ is the Prandtl number of air. The heat liberation rate at the liquid–gas interface due to condensation, q_L , is given by $q_L = \rho_a h_m h_{fg}(\omega_\infty - \omega_i)$, where ρ_a is the density of air, h_m is the mass transfer coefficient, and ω_∞ and ω_i are the mass fraction of moisture in bulk air and at the gas–liquid interface, respectively. Since the Lewis number, defined as $Le = \alpha/D$ with D being the mass diffusivity is near unity for humid air,⁴¹

$$q_L \approx \frac{h_v h_{fg}}{c_p} (\omega_\infty - \omega_i) \quad (10)$$

where c_p is the specific heat of dry air at constant pressure. The moisture fractions ω_i and ω_w depend on the interface temperature as⁴²

$$\omega_j = 3.7444 \times 10^{-3} + 0.3078 \times 10^{-3} T_j + 0.0046 \times 10^{-3} T_j^2 + 0.0004 \times 10^{-3} T_j^3 \quad (11)$$

where $j = i$ or w and T is in °C. The conduction heat transfer rate, q_d , is given by

$$q_d = \frac{k_l}{\delta} (T_i - T_w) \quad (12)$$

where the film thickness δ is estimated by the Nusselt theory that balances the viscous shear force and the gravitational force:⁴³

$$\delta \approx \left[\frac{4k\mu_l(T_s - T_w)L}{g\rho(\rho - \rho_a)h_{fg}} \right]^{1/4} \quad (13)$$

where μ_l is the viscosity of liquid. Combining eqs 8–13, we first find that $\omega_i \approx \omega_w$ within 0.25% error owing to a very small film thickness (85 μm). Then eq 10 gives the condensation rate, $\dot{m} = q_d A / h_{fg}$, with A being the area of the condensation substrate, as $\dot{m} = 0.245$ g/h. This favorably agrees with the measured value of 0.22 g/h, corresponding to the hatched bar of surface III in Figure 5a.

B. Effective Drainage. Although the hydrophilic surface III has been revealed to exhibit the highest water collection and condensation rates, the drainage ratio k is below 0.8 due to the puddle formed at the bottom. The puddle blocks the effective drainage of water down to the container. Therefore, we tested various designs of hydrophilic condensation surface to enhance the drainage ratio as shown in Figure 7a. The lower portion of the surface was patterned using a method of Figure 2a so that the superhydrophilic area that guides the water film is surrounded by the superhydrophobic area. We used nanostructured superhydrophilic surfaces with long-lasting hydrophilicity instead of smooth surfaces that maintain hydrophilicity for too short a time (a few minutes) to be patterned subsequently. Surface A is an entirely superhydrophilic square with 30 mm in sidelength. Surface B has a triangular superhydrophilic area with the angle at the lower vertex 124°. Surface C has a narrow straight lane or drainage path, 1 mm wide and 4 mm long, connected with a triangle of the diverging angle 150°. Surfaces D and E have an 8 mm-long straight lane with 1 mm and 2 mm in width, respectively. To focus on the retention and drainage characteristics of those surfaces, we supplied water on the vertically situated substrate with a syringe. We measured the weight of water that drains into a container and that of the water remaining on the surface. Here the water retention is defined as the capacity of a surface to hold water on it. Then the minimum water retention is the weight of the water remaining on the surface right after the falloff of a drop. The maximum water retention is obtained by adding the weight of the drop falling off the surface to that of the remaining water. The lower the retentions, the more effective is the drainage.

Figure 7b shows the images of the water film on the lower portion of the substrate. Surface A forms a puddle as delineated above, which sheds a big drop of 0.150 g while holding water film of 0.086 g on its surface. On surface B, a triangular puddle is formed following the edge of the hydrophilic region.

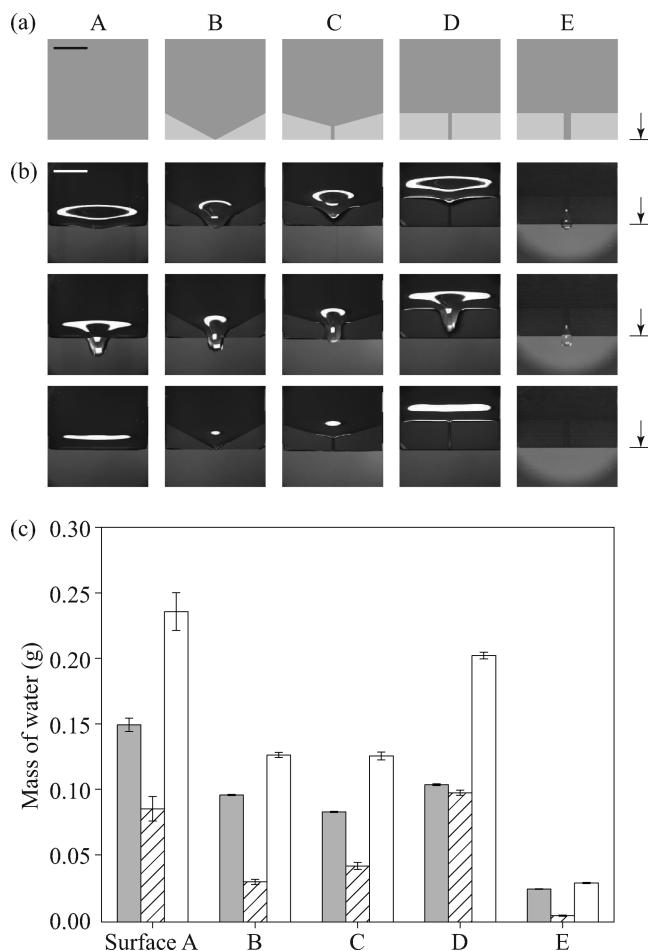


Figure 7. (a) Various designs of the condensation surface to enhance drainage. (b) Images of the water flow on each surface. The arrows indicate the location of the plate bottom. Scale bar: 10 mm. (c) Weight of a droplet (gray bar), minimum retention (hatched bar), maximum retention (empty bar) of each surface.

Although the drainage is improved as compared with that of surface A, the puddle is not completely removed as shown in Figure 7c. Liquid on surface C shows a similar behavior to that on surface B. The puddle is still maintained above the drainage path which is too narrow to overcome the surface tension of water. Surface D helps the water film to converge, and sheds drops of 0.104 g per drop, smaller than those from the puddle of surface A. However, a large puddle still remains before the narrow lane thus its water retentions are greater than those of surfaces B and C. On surface E, no puddle is formed as the water film is continuously guided toward the tip of the path. Small droplets of 0.025 g per drop are shed leaving little water on the surface. These observations lead us to conclude that a drainage path with an appropriate width can minimize the water hold-up, or maximize the drainage efficiency. The minimum and maximum retention of surface E is respectively 5.4% and 12.6% of that of surface A.

On the basis of this finding, we searched for the optimal dimensions, i.e., width and length, of a drainage path. It is necessary to minimize the path length while maintaining a high drainage ratio to maximize the water collection. Straight paths of variable width $w \in [1\ 3]$ mm and length $l \in [2\ 10]$ mm were tested. We found that when $w \leq 2$ mm, water does not spontaneously wet the drainage path; thus, a puddle remains.

See Figure 8a. It is because the undulation on the puddle with the wavelength shorter than 2 mm is stabilized by the surface

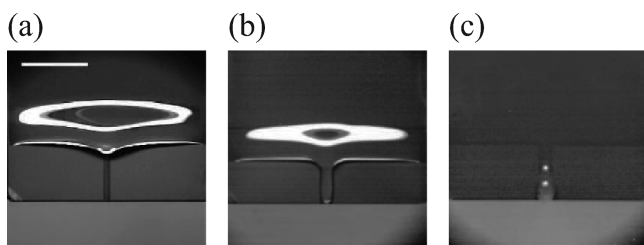


Figure 8. (a) Puddle residing above the hydrophilic lane of $w = 1$ mm. (b) Puddle remaining on the lane of $w = 2$ mm and $l = 6$ mm. (c) Narrow stream of water guided by the lane with $w = 2$ mm and $l = 8$ mm achieving effective drainage. Scale bar, 10 mm.

tension even under a gravitational field. If w is too wide (~ 3 mm), the water film on the lane forms another puddle instead of being effectively drained. For $w \geq 2$ mm, the lane length should be greater than the critical length $l_c = 8$ mm for a puddle to drain into the straight path. Otherwise, the downward flow along the lane is not strong enough to fully destabilize the puddle thus the puddle remains as shown in Figure 8b. It was also found that as long as $l \geq l_c$, the weight of a droplet that falls off the surface is independent of l . Therefore, the optimal path dimensions to achieve effective water drainage are such that $w \in [2-2.5]$ mm and $l = 8$ mm. It is interesting to note that the optimal range of the width favorably agrees with the capillary length of water, $[\sigma/(\rho g)]^{1/2} = 2.7$ mm, a length scale at which capillary and gravitational forces are balanced.

To verify the effects of the drainage path in water harvest, we compared the rates of water collection and condensation of the surface having a drainage path of $w = 2$ mm and $l = 8$ mm (surface E) with those of the uniformly superhydrophobic (I), smooth hydrophilic (III), and superhydrophilic surface (IV or A). The total area of surface E including both superhydrophilic and superhydrophobic regions is identical to the area of the other surfaces (I, III, and IV). The condensation experiments reveal that surface E has the superior water collection efficiency as shown in Figure 9. The water collection rate of surface E is 9.8% and 48.6% higher than that of surfaces III and IV, respectively, owing to enhanced drainage ratio by 15.5% and

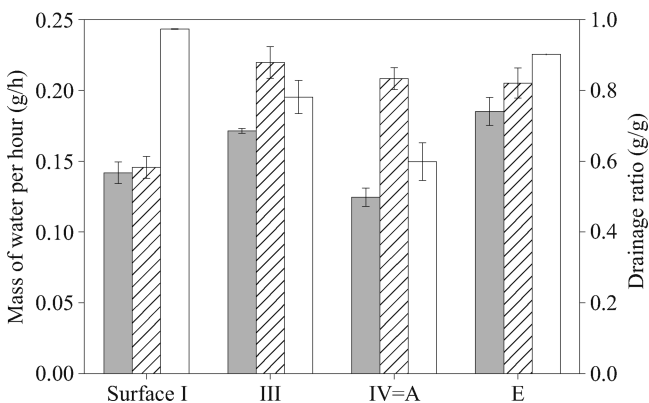


Figure 9. Water collection rate (gray bar), condensation rate (hatched bar), and drainage ratio (empty bar) of a uniformly superhydrophobic (I), hydrophilic (III), and superhydrophilic surface (IV = A) and a surface with the drainage path (E).

50.7%, respectively. The water collection rate of surface E is much higher (by 30.5%) than that of surface I despite the slightly lower drainage ratio because of superior condensation rate of superhydrophilic surfaces to that of superhydrophobic surfaces. We note that although surface IV has a hydrophilic area 33.1% greater than surface E, both the surfaces have similar condensation rates. This is because the hydrophilic area of surface E is covered with thin water film of low thermal resistance but surface A is covered with a thick puddle near its bottom having high thermal resistance. Therefore, the drainage path does not only provide an effective water exit but also compensates the reduction of hydrophilic area by eliminating a puddle with a high thermal resistance.

IV. CONCLUSIONS

We have investigated the effects of surface wettability on the rate of water harvest via vapor condensation. The rates of vapor condensation and subsequent water drainage on vertical surfaces of a wide range of wettability have been quantified, which have been seldom investigated thus far. In contrast to previous reports specific to fog basking, here we showed that a uniformly hydrophilic surface has higher rates of water condensation and collection than a uniformly hydrophobic surface and a surface with hydrophilic patches in hydrophobic background, when dewing occurs in still air. This observation is consistent with the fact that the moisture-harvesting Australian frogs and lizards have uniformly hydrophilic skins unlike the fog-basking beetles of the Namib Desert with hydrophobic integument. We quantified a crucial influence of drainage on water collection rates and determined the condition for a puddle formed at the lower edge of the hydrophilic substrate to fall, for the first time. A thin hydrophilic lane at the lower portion of the condensation substrate was shown to greatly enhance water drainage and consequently water collection rates. The optimal geometry of the drainage path was identified through the experiments.

In a practical device where the size of the condensation substrate should be large, multiple paths would be required. Although we anticipate minimal change of the optimal design, the number and spacing of the paths need to be determined when the width of the condensation substrate increases. Our preliminary tests reveal that increasing the number of drainage paths for the current size of substrate does not alter the water collection performance. Analysis of thin film flows near the edge of the substrate is required to explain the optimal width and length of the drainage path and to predict the optimal spacing between the multiple paths for large substrates. The condensation and drainage behavior of water on cold surfaces that we have investigated here can guide a design of a practical water-harvesting device, which has started to be implemented in some tropical regions.^{44,45} In particular, the analytical methods adopted in this work to estimate various parameters associated with water harvesting, e.g., the volume of drops and puddles that are shed off the surface, growth rate of a drop via condensation, and rate of film condensation from unsaturated air, will serve as useful tools in such an application. Also our study helps one to understand the water-collection mechanism of the frogs and lizards that live in the Australian desert.

■ AUTHOR INFORMATION

Corresponding Author

*E-mail: hyk@snu.ac.kr.

Notes

The authors declare no competing financial interest.

ACKNOWLEDGMENTS

This work was supported by KIST, Ministry of Knowledge Economy (Global Excellent Technology Innovation R&D Program) and National Research Foundation (Grant Nos. 2011-0030744 and 2012-008023) of the Republic of Korea, and administered via SNU-IAMD.

REFERENCES

- (1) Rosegrant, M. W.; Cai, X.; Cline, S. A. *Global Water Outlook to 2025: Averting an Impending Crisis*; International Food Policy Research Institute: Washington, DC, 2002.
- (2) Shiklomanov, I. A. Appraisal and Assessment of World Water Resources. *Water Int.* **2000**, *25*, 11–32.
- (3) Hamilton, W. J. Fog Basking by the Namib Desert Beetle *Onymacris unguicularis*. *Nature* **1976**, *262*, 284–285.
- (4) Parker, A. R.; Lawrence, C. R. Water Capture by a Desert Beetle. *Nature* **2001**, *414*, 33–34.
- (5) Zhai, L.; Berg, M. C.; Cebeci, F. C.; Kim, Y.; Milwid, J. M.; Rubner, M. F.; Cohen, R. E. Patterned Superhydrophobic Surfaces: Toward a Synthetic Mimic of the Namib Desert Beetle. *Nano Lett.* **2006**, *6*, 1213–1217.
- (6) Garrod, R. P.; Harris, L. G.; Schofield, W. C. E.; McGettrick, J.; Ward, L. J.; Teare, D. O. H.; Badyal, J. P. S. Mimicking a Stenocara Beetle's Back for Microcondensation Using Plasmachemical Patterned Superhydrophobic-Superhydrophilic Surfaces. *Langmuir* **2007**, *23*, 689–693.
- (7) Dorrer, C.; Rühle, J. Mimicking the Stenocara Beetle: Dewetting of Drops from a Patterned Superhydrophobic Surface. *Langmuir* **2008**, *24*, 6154–6158.
- (8) Nørgaard, T.; Dacke, M. Fog-Basking Behaviour and Water Collection Efficiency in Namib Desert Darkling Beetles. *Front. Zool.* **2010**, *7*, 23–30.
- (9) Tracy, C. R.; Laurence, N.; Christian, K. A. Condensation onto the Skin as a Means for Water Gain by Tree Frogs in Tropical Australia. *Am. Nat.* **2011**, *178*, 553–558.
- (10) Gans, C.; Merlin, R.; Blumer, W. F. C. The Water-Collecting Mechanism of *Moloch horridus* Re-Examined. *Amphibia-Reptilia* **1982**, *3*, 57–64.
- (11) Comanns, P.; Effertz, C.; Hischen, F.; Staudt, K.; Böhme, W.; Baumgartner, W. Moisture Harvesting and Water Transport through Specialized Micro-structures on the Integument of Lizards. *Beilstein J. Nanotechnol.* **2011**, *2*, 204–214.
- (12) Kuvannarat, T.; Wang, C.-C.; Wongwises, S. Effect of Fin Thickness on the Air-Side Performance of Wavy Fin-and-Tube Heat Exchangers under Dehumidifying Conditions. *Int. J. Heat Mass Transf.* **2006**, *49*, 2587–2596.
- (13) Ma, X.; Ding, G.; Zhang, Y.; Wang, K. Effects of Hydrophilic Coating on Air Side Heat Transfer and Friction Characteristics of Wavy Fin and Tube Heat Exchangers under Dehumidifying Conditions. *Energy Convers. Manage.* **2007**, *48*, 2525–2532.
- (14) Wang, C.-C.; Chang, C.-T. Heat and Mass Transfer for Plate Fin-and-Tube Heat Exchangers, With and Without Hydrophilic Coating. *Int. J. Heat Mass Transfer* **1998**, *41*, 3109–3120.
- (15) Wang, C.-C.; Lee, W.-S.; Sheu, W.-J.; Chang, Y.-J. A Comparison of the Airside Performance of the Fin-and-Tube Heat Exchangers in Wet Conditions; With and Without Hydrophilic Coating. *Appl. Therm. Eng.* **2002**, *22*, 267–278.
- (16) Hong, K.; Webb, R. L. Performance of Dehumidifying Heat Exchangers With and Without Wetting Coatings. *J. Heat Transfer* **1999**, *121*, 1018–1026.
- (17) Ma, X.; Ding, G.; Zhang, Y.; Wang, K. Airside Heat Transfer and Friction Characteristics for Enhanced Fin-and-Tube Heat Exchanger with Hydrophilic Coating under Wet Conditions. *Int. J. Refrigeration* **2007**, *30*, 1153–1167.
- (18) Ma, X.; Ding, G.; Zhang, Y.; Wang, K. Airside Characteristics of Heat, Mass Transfer and Pressure Drop for Heat Exchangers of Tube-in-Hydrophilic Coating Wavy Fin under Dehumidifying Conditions. *Int. J. Heat Mass Transfer* **2009**, *52*, 4358–4370.
- (19) American Society of Refrigerating Engineers. *2005 ASHRAE Handbook*; ASHRAE: Atlanta, GA, 2005.
- (20) Carey, V. P. *Liquid-Vapor Phase-Change Phenomena*; Hemisphere: Washington, DC, 1992.
- (21) Kim, G.-R.; Lee, H.; Webb, R. L. Plasma Hydrophilic Surface Treatment for Dehumidifying Heat Exchangers. *Exp. Thermal Fluid Sci.* **2002**, *27*, 1–10.
- (22) Lara, J. R.; Holtzapfel, M. T. Experimental Investigation of Dropwise Condensation on Hydrophobic Heat Exchangers Part I: Dimpled-Sheets. *Desalination* **2011**, *278*, 165–172.
- (23) Narhe, R. D.; Beysens, D. A. Growth Dynamics of Water Drops on a Square-Pattern Rough Hydrophobic Surface. *Langmuir* **2007**, *23*, 6486–6489.
- (24) Varanasi, K.; Hsu, M.; Bhate, N.; Yang, W.; Deng, T. Spatial Control in the Heterogeneous Nucleation of Water. *Appl. Phys. Lett.* **2009**, *95*, 094101.
- (25) Tadmor, R.; Yadav, P. S. As-placed Contact Angles for Sessile Drops. *J. Colloid Interface Sci.* **2008**, *317*, 241–246.
- (26) de Gennes, P.-G.; Brochard-Wyart, F.; Quéré, D. *Capillarity and Wetting Phenomena: Drops, Bubbles, Pearls, Waves*; Springer: New York, 2004.
- (27) Hegemann, D.; Brunner, H.; Oehr, C. Plasma Treatment of Polymers to Generate Stable, Hydrophobic Surfaces. *Plasmas Polym.* **2001**, *6*, 221–235.
- (28) Cha, T.-G.; Yi, J. W.; Moon, M.-W.; Lee, K.-R.; Kim, H.-Y. Nanoscale Patterning of Microtextured Surfaces to Control Superhydrophobic Robustness. *Langmuir* **2010**, *26*, 8319–8326.
- (29) Lee, M.; Chang, Y. S.; Kim, H.-Y. Drop Impact on Microwetting Patterned Surfaces. *Phys. Fluids* **2010**, *22*, 072101.
- (30) Corbella, C.; Bialuch, I.; Kleinschmidt, M.; Bewilogua, K. Upscaling the Production of Modified a-C:H Coatings in the Framework of Plasma Polymerization Processes. *Solid State Sci.* **2009**, *11*, 1768–1772.
- (31) Yi, J. W.; Moon, M.-W.; Ahmed, S. F.; Kim, H.; Cha, T.-G.; Kim, H.-Y.; Kim, S.-S.; Lee, K.-R. Long-Lasting Hydrophilicity on Nanostructured Si-Incorporated Diamond-Like Carbon Films. *Langmuir* **2010**, *26*, 17203–17209.
- (32) Furmidge, C. G. L. Studies at Phase Interfaces. I. The Sliding of Liquid Drops on Solid Surfaces and a Theory for Spray Retention. *J. Colloid Sci.* **1962**, *17*, 309–324.
- (33) Kim, H.-Y.; Lee, H. J.; Kang, B. H. Sliding of Liquid Drops Down an Inclined Solid Surface. *J. Colloid Interface Sci.* **2002**, *247*, 372–380.
- (34) Cho, H.; Kim, H.-Y.; Kang, J. Y.; Kim, T. S. How the Capillary Burst Microvalve Works. *J. Colloid Interface Sci.* **2007**, *306*, 379–385.
- (35) Kim, S.; Kim, K. J. Dropwise Condensation Modeling Suitable for Superhydrophobic Surfaces. *J. Heat Transfer* **2011**, *133*, 081502.
- (36) Tanasawa, I. Advances in Condensation Heat Transfer. *Adv. Heat Transfer* **1991**, *21*, 55–139.
- (37) Rose, J. W. Dropwise Condensation Theory. *Int. J. Heat Mass Transfer* **1981**, *24*, 191–194.
- (38) Minkowycz, W. J.; Sparrow, E. M. Condensation Heat Transfer in the Presence of Noncondensables, Interfacial Resistance, Superheating, Variable Properties, and Diffusion. *Int. J. Heat Mass Transfer* **1966**, *9*, 1125–1144.
- (39) Volmer, M.; Weber, A. Keimbildung in übersättigten Gebilden. *Z. Phys. Chem.* **1926**, *119*, 277–301.
- (40) Churchill, S. W.; Chu, H. H. S. Correlating Equations for Laminar and Turbulent Free Convection From a Vertical Plate. *Int. J. Heat Mass Transfer* **1975**, *18*, 1323–1329.
- (41) Coney, J. E. R.; Sheppard, C. G. W. Fin Performance with Condensation from Humid Air: a Numerical Investigation. *Int. J. Heat and Fluid Flow* **1989**, *10*, 224–231.

(42) Kundu, B. Approximate Analytic Solution for Performances of Wet Fins with a Polynomial Relationship between Humidity Ratio and Temperature. *Int. J. Therm. Sci.* **2009**, *48*, 2108–2118.

(43) Incropera, F. P.; DeWitt, D. P. *Fundamentals of Heat and Mass Transfer*, 5th ed.; Wiley: Hoboken, NJ, 2002.

(44) Clus, O.; Ortega, P.; Muselli, M.; Milimouk, I.; Beysens, D. Study of Dew Water Collection in Humid Tropical Islands. *J. Hydrology* **2008**, *361*, 159–171.

(45) Sharan, G.; Clus, O.; Singh, S.; Muselli, M.; Beysens, D. A Very Large Dew and Rain Ridge Collector in the Kutch Area (Gujarat, India). *J. Hydrology* **2011**, *405*, 171–181.